Transform Coding in the VVC Standard

Xin Zhao, *Senior Member, IEEE*, Seung-Hwan Kim, Yin Zhao, Hilmi E. Egilmez, *Member, IEEE*, Moonmo Koo, Shan Liu, *Senior Member, IEEE*, Jani Lainema, and Marta Karczewicz

(Invited Paper)

***Abstract*— In the past decade, the development of transform coding techniques has achieved significant progress and several advanced transform tools have been adopted in the new generation Versatile Video Coding (VVC) standard. In this paper, a brief history of transform coding development during VVC standardization is presented, and the transform coding tools in the VVC standard are described in detail together with their initial design, incremental improvements and implementation aspects. To improve coding efficiency, four new transform coding techniques are introduced in VVC, which are namely Multiple Transform Selection (MTS), Low-Frequency Non-separable Secondary Transform (LFNST) and Sub-Block Transform (SBT), as well as a large (64-point) type-2 DCT. The experimental results on VVC reference software (VTM-9.0) show that average 4.5% and 3.6% overall coding gain can be achieved by the VVC transform coding tools for All Intra and Random Access configurations, respectively.**

***Index Terms*— Versatile video coding (VVC), joint video exploration team (JVET), transform coding, MTS, LFNST, SBT, VVC test model (VTM), joint exploration model (JEM).**

I. Introduction

TRANSFORM coding has been an essential part of many practical video codecs for achieving a high compression ratio, and it has been successfully adopted in multiple video coding standards, e.g., H.261 [1], MPEG-1 [2], MPEG-2 [3], H.263 [4], H.264/AVC [5] and High-Efficiency Video Coding (HEVC) [6]. The development of transform coding in the past several decades was based on the traditional DCT, more specifically, type-2 DCT (DCT-2) [7], due to its reasonable tradeoff between coding performance and complexity. Under the first-order Markov conditions, which efficiently model the characteristics of natural imagery sources, it has been mathematically proved that DCT-2 approximates the optimal data-driven Karhunen-Loève transform (KLT) [8]. Fast method for implementing DCT-2 was first proposed in [9] and further developed in the following decades. In H.264/AVC, a low-complexity 4×4 transform [10] is adopted featured by multiplier-less calculation, fixed-point and 16-bit intermediate data representation. In addition, a secondary 4×4 Hadamard transform can be applied in H.264/AVC to further decorrelate DC coefficients of 4×4 transform block. In HEVC, the transform size of DCT-2 is further extended to 8×8, 16×16 and 32×32 with fixed-point transform kernels, and the implementations can be done using either direct matrix multiplication or a partial butterfly fast method. In addition, 16-bit intermediate data representation and arithmetic is kept in the HEVC transform design [11]. Moreover, in HEVC, a 4×4 DST-7 is applied for 4×4 intra prediction residuals. Further technical advances on top of DCT-2 are mainly reflected by the extended transform sizes and different designs of integer DCT-2 kernels. In [12], a directional extension of conventional DCT-2 was proposed, which employs two 1-D DCTs along directional directions rather than the horizontal and vertical directions. In recent years, driven by the drastically increased traffic of multimedia communications and new systems supporting more computational power, extensive efforts have been made to seek for higher coding performance at an increased yet feasible complexity cost.

From the industrial standardization side, the Joint Video Exploration Team (JVET) was created in 2015 as a joint effort of ITU-T SG 16 WP 3 and ISO/IEC JTC 1/SC 29/WG 11 to explore advanced video coding technologies beyond HEVC. In 2018, after receiving 23 responses to the Call for Proposal (CfP) on next-generation video coding, the Joint Video Experts Team, also known as JVET, was created that officially launched the standardization of the new generation Versatile Video Coding (VVC) [13]. After two years of development, VVC has been finalized in July 2020 with a substantial objective coding gain over its predecessor, HEVC.

This paper provides a history of the tool development in transform coding and presents how these tools are shaped into their final designs in VVC. Among all the coding tools included in VVC, the major advances in transform coding techniques can be categorized into primary transform, secondary transform and transform partitioning, which are summarized in the following three subsections.

The remainder of this paper is organized as follows. In Section II, further development of transform coding beyond HEVC is reviewed in three categories, including 1) primary transform, 2) secondary transform and 3) transform partitioning. In Section III, the transform design in VVC is described with technical details, and the encoder implementations on

Manuscript received August 23, 2020; revised February 15, 2021 and April 14, 2021; accepted May 28, 2021. Date of publication June 9, 2021; date of current version October 4, 2021. This article was recommended by Associate Editor J. Boyce. *(Corresponding authors: Xin Zhao; Seung-Hwan Kim.)*

Xin Zhao and Shan Liu are with Tencent Media Lab, Palo Alto, CA 94306 USA (e-mail: xinzzhao@tencent.com).

Seung-Hwan Kim is with LG Electronics, San Diego, CA 92131 USA (e-mail: seunghwan3.kim@lge.com).

Yin Zhao is with Huawei Technologies, Hangzhou 310057, China.

Hilmi E. Egilmez and Marta Karczewicz are with Qualcomm Technologies Inc., San Diego, CA 92121 USA.

Moonmo Koo is with LG Electronics, Seoul 06772, South Korea.

Jani Lainema is with Nokia Technologies, 33101 Tampere, Finland.

Color versions of one or more figures in this article are available at https://doi.org/10.1109/TCSVT.2021.3087706.

Digital Object Identifier 10.1109/TCSVT.2021.3087706

top of version 9.0 of the VVC reference software called VVC Test Model (VTM) are described in Section IV. Complexity analysis and experimental results are discussed in Section V and Section VI, respectively, and Section VII concludes this paper.

II. Review of Transform Coding Tools Beyond HEVC

A. Primary Transform

The fixed transform scheme based on DCT-2 has been widely used in the past video coding standards. However, due to diverse characteristics of image/video content, it is not always efficient to use a single transform kernel for all prediction residuals. In [14], it is proposed to use sine and cosine transforms alternatively for image coding. In [15], mode-dependent directional transforms (MDDTs) are proposed for intra prediction residuals, wherein hard-coded KLTs are selected as the horizontal and vertical transform based on intra prediction mode. Moreover, with a first-order Gauss-Markov model for image pixels, it was further mathematically proved in [16] that, the optimal horizontal (vertical) transform applied on the intra prediction residual of horizontal (vertical) prediction mode is actually DST-7. In HEVC, a 4×4 DST-7 is applied for 4×4 intra prediction residuals, and better coding performance is achieved over DCT-2. Furthermore, to overcome the limitation of using single fixed kernel, transform signaling has been proposed, which allows multiple options of transform kernels, so that an encoder can choose a transform on a per block basis and signal such that selection in the bitstream. In such signaling schemes, transform candidates can be derived by off-line training or selected from a group of mathematically defined transforms, such as the DCT/DST families [17].

Multiple transform selection with transform signalling was proposed in [18] as known as rate-distortion optimized transform (RDOT), which applies multiple Karhunen-Loève transforms (KLTs) and the transform selection is rate-distortion optimized. Alternative schemes that apply DCT/DST as the transform candidates are also proposed in [19]–[21]. More specifically, in [20], an Enhanced Multiple Transform (EMT) scheme was proposed and included in the Joint Exploration Model, which applies intra prediction mode dependent transform sets with each set consist of multiple candidates of transform kernels. Moreover, multiple non-separable transform schemes have also been proposed in [22], [23]. In [24], a row-column transform scheme is proposed, which approximates non-separable KLT using a separable transform.

B. Secondary Transform

Secondary transform refers to an additional transform process that follows the primary transform. In H.264/AVC, a 16×16 transform is implemented as sixteen 4×4 transforms, and the DC coefficients of each 4×4 transform block are combined as one 4×4 block and further processed using a secondary Hadamard transform [5]. During the development of HEVC, a secondary rotational transform (ROT) [25] was proposed on top of DCT, with kernels featured by sparse transform matrices constructed using pre-defined Givens rotations. Note that ROT is still a separable transform and the coding gain overlaps with the DST-7. In HEVC, 4×4 DST-7 has been adopted for intra coding with a simpler design.

Non-separable transform schemes have been proposed as a secondary transform [26], namely Non-Separable Secondary Transform (NSST) as either a direct matrix multiply [26] or Hypercube-Givens Transform (HyGT) [27] where transform could be represented as multi-layer transforms by cascaded Givens rotations in a hypercube arrangement. The major benefit of applying non-separable transform as a secondary transform is to achieve a better tradeoff between coding efficiency and complexity. With NSST, a non-separable secondary transform is performed on the lower-frequency coefficients so that computational complexity for non-separable transform is largely reduced. Besides, HyGT provides parallel, multi-stage decompositions for non-separable transforms with lower computational complexity and memory cost, yet it introduces additional latency due to its stage-wise implementations.

C. Transform Partitioning

Transform coding is applied to reduce the statistical dependency among residual samples. However, when the residual samples are distributed locally, applying a larger transform may create high frequencies that can be expensive for entropy coding. To address this issue, transform partitioning schemes have been proposed. In [28], adaptive block-size transforms (ABT) was proposed, and the basic idea of inter ABT is to align the block size used for transform coding of the prediction error to the block size used for motion compensation In HEVC, a quadtree partitioning scheme has been applied for transform [29], and a spatially varying transform (SVT) was proposed in [30] to adapt the position and size of transform with localized residual samples.

III. Transform Design in VVC

Transform design in VVC mainly includes three aspects: the primary transform, secondary transform and transform partitioning. In this section, the new transform coding tools in VVC are described with respect to each of the three aspects. In this paper, an N-point transform refers to a one-dimensional transform that can be applied on an N-point input vector, which is done using a transform matrix of size N by N.

Several design aspects of HEVC transform coding are inherited in VVC, including: 1) fixed-point operations are used and intermediate data representation and arithmetic is kept to be 16-bit, 2) the transform process can be either implemented using direct matrix multiply or a fast method, e.g., partial butterfly, 3) the transform kernels are designed by scaling the transform basis with $64\sqrt{N}$ and rounding to the nearest integer with minor adjustment, where the norm of transform basis is 1 and N is the transform size, 4) smaller DCT-2 is part of the larger DCT-2, so all DCT-2 kernels are embedded in the 64×64 DCT-2 transform kernel. Although up to 128×128 coding block sizes can be applied in VVC, the transform coding is designed to be compatible with the virtual pipeline

data units (VPDUs) implementation. In hardware decoding process, VPDUs are non-overlapping 64 × 64 blocks and consecutive VPDUs are processed in parallel by multiple pipelines.

A. Primary Transform

1) Transform Kernels: In VVC, in addition to the conventional type-2 DCT (DCT-2), alternate transform types, including type-7 DST (DST-7) and type-8 DCT (DCT-8), are employed. The basic functions of DST-7 and DCT-8 are formulated in below Equation (1) and (2), respectively.

$$T_i(j) = \sqrt{\frac{4}{2N+1}} \cdot \sin\left(\frac{\pi \cdot (2i+1) \cdot (j+1)}{2N+1}\right), \quad (1)$$

$$T_i(j) = \sqrt{\frac{4}{2N+1}} \cdot \cos\left(\frac{\pi \cdot (2i+1) \cdot (2j+1)}{4N+2}\right), \quad (2)$$

where N is the transform size, $i = 0, 1, \ldots, N-1$ refers to the element index of the output vector, and $j = 0, 1, \ldots, N-1$ refers to the element index of the input vector. For uneven distribution of residual, DST-7 and DCT-8 are usually more efficient than DCT-2 since their basis functions are more aligned with such statistics [20]. The size of DCT-2 ranges from 4-point to 64-point, and DST-7/DCT-8 ranges from 4-point to 32-point. It is noted that the transform bases of DST-7 and DCT-8 are flipped versions of each other with alternating sign changes.

The transform kernels defined in VVC are composed of 8-bit signed integers and all the primary transform kernels in HEVC, including 4-point DST-7 and DCT-2 ranging from 4-point to 32-point, are kept unchanged. The additional integer transform kernels defined in VVC are derived by scaling the floating-point transform kernel with $64\sqrt{N}$, where N is the transform size, and further adjusted by ± 1 after rounding. The adjustment of 64-point DCT-2 is performed in a way that all the DCT-2 kernel defined in HEVC are included, partial butterfly [11] is supported and kernel elements are optimized towards better orthogonality. The adjustment of kernel element is performed with the following criteria: 1) to align with the HEVC core transform design that smaller DCT-2 can be extracted as part of the larger DCT-2, only 32 elements can be adjusted and the remaining 33 elements are kept same as HEVC to generate smaller DCT-2 from 4×4 to 32×32, 2) the orthogonality is optimized such that $K \times K^{\mathrm{T}}$ is as close as possible to the identity matrix, wherein K is the transform matrix, 3) the adjustment can be done only with offset -1 and $+1$ to ensure that the decorrelation capability of adjusted transform kernel approximates DCT-2 efficiently. The adjustment of DST-7/DCT-8 kernels are performed to ensure the three notable features associated with DST-7/DCT-8, as illustrated in Figure 1, including feature 1) repetitive segments $\{b, f, i, l, o\}$ in some bases, 2) unique coefficient value in one basis and 3) mathematical relationship among coefficients in a tuple with fixed pattern in some bases, as pointed out in [32], [33], are kept in the integer kernel with optimized orthogonality. Specially, for feature 3),

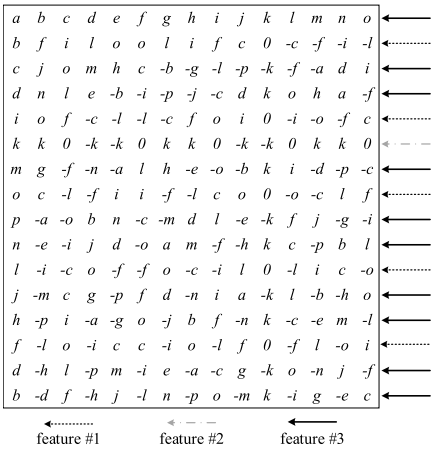

Fig. 1. Illustration of three features in the 16 × 16 DST-7 transform matrix of VVC.

the following formulation is supported:

$$\begin{aligned} a + j &= l \\ b + i &= m \\ c + h &= n \\ d + g &= o \\ e + f &= p \end{aligned} \quad (3)$$

To align the worst-case multiplications per coefficient with HEVC, for 64-point DCT-2 and 32-point DST-7/DCT-8, only the first 32 and 16 low-frequency coefficients are kept, respectively, and the high frequency coefficients are zeroed out, which is also considered in last coefficient position coding and coefficient group scanning [31]. More details will be discussed in the Section V. Moreover, based on the three features of the DST-7/DCT-8 kernels, a fast transform scheme with support of dual implementations is included in VVC [32], [33]. In this way, the fast algorithm and direct matrix multiply produce identical results. Meanwhile, the fast method achieves around 50% multiplication reduction for 16-point DST-7/DCT-8 [32].

In VVC, the primary transform is specified as separable transform. Five different combinations of transform types are supported, including the conventional (DCT-2, DCT-2) and four new MTS mode combinations, i.e., (DST-7, DST-7), (DST-7, DCT-8), (DCT-8, DST-7) and (DCT-8, DCT-8). The explicit combination between DCT-2 and DST-7 (or DCT-8) with extra signalling overhead is not supported due to the limited coding gain and increased complexity for introducing extra encoder search and additional transform combinations. In VVC, DST-7 and DCT-8 can be applied to the luma blocks in several coding tools, including Multiple Transform Selection (MTS), Intra Sub-Partitioning (ISP) [34] and Sub-block Transform (SBT), which will be detailed in the following subsection related to transform type selection. For chroma coding, the potential benefits of DST-7/DCT-8 have also been studied during the development of VVC. However, since chroma components typically present smooth textures, where DCT-2 is sufficient, the coding gain versus complexity tradeoff is less beneficial.

2) Multiple Transform Selection: In VVC, there are two variants of Multiple Transform Selection (MTS), called

TABLE I
SPECIFICATION OF TRANSFORM KERNELS DEPENDING ON THE SYNTAX

mts_idx	0	1	2	3	4
trTypeHor	DCT-2	DST-7	DCT-8	DST-7	DCT-8
trTypeVer	DCT-2	DST-7	DST-7	DCT-8	DCT-8

TABLE II
SUMMARY OF THE COMBINATIONS OF DIFFERENT TOOLS

Tools		MIP	ISP
MTS	Explicit intra MTS	Y	N
	Explicit inter MTS	N/A	N/A
	Implicit MTS	N	Y
LFNST		Partially (see section III-B)	Y
SBT		N/A	N/A

explicit and implicit MTS. The explicit MTS can be applied to both intra and inter coded blocks, while the implicit MTS can be only used for intra coded blocks. In explicit MTS, the choice of DST-7/DCT-8 is indicated by explicit signaling of the transform type. In implicit MTS, the transform type are selected based on coded information that is known to both the encoder and decoder, and transform type signalling is not needed. In the Sequence Parameter Set (SPS), there are three flags controlling MTS operation. The first is used to enable MTS itself. The second is used to select between explicit or implicit intra MTS and the last is used to enable explicit inter MTS. Thus, with the latter two flags, four MTS mode combinations need to be selected if MTS is enabled. In explicit MTS, the index mts_idx is signaled at the end of Coding Unit (CU) level syntax to indicate the transform type for horizontal transform (trTypeHor) and vertical transform (trTypeVer). The value of mts_idx ranges from 0 to 4, and the mapping to the transform type is specified in Table I.

The MTS index, denoted as mts_idx, is signalled only when nonzero coefficients for luma block exist beyond the DC coefficient and nonzero coefficient is not identified outside the top-left 16×16 coefficients region, since DST-7/DCT-8 has only an impact on the lowest 16×16 frequency coefficients. In other words, identification of a nonzero coefficient beyond the lowest 16×16 coefficients means DST-7/DCT-8 not being applied. In addition, when several tools are enabled, including ISP, SBT and Low-Frequency Non-Separable Transform (LFNST), mts_idx is not signaled [35] and transform type is inferred as either DCT-2 or a pre-defined transform type. In Table II, the combinations of different tools, including MTS, LFNST, MIP, ISP and SBT, have summarized, where "Y/N" means the associated coding tools in the row and column can/cannot be combined, and "N/A" means the associated combination is not applicable.

The initial design of implicit MTS was first proposed in [36] where the transform types were derived based on the shape of the coded block. The transform type selection condition has later been simplified in [37] and led to the final design of implicit MTS in VVC. That is, DST-7 is applied as the horizontal (vertical) transform if block width (height) is smaller than 32. Otherwise, DCT-2 is used. This same rule is also used to derive transforms for ISP coded blocks. In Figure 2, examples of implicit MTS derivation are illustrated for different block sizes. The implicit MTS design in VVC can be viewed as an extension of the HEVC transform derivation for intra prediction residual, by extending the applicable block size for DST-7 from 4×4 to 16×16 (inclusive) and other rectangular block sizes in between. Other than the restrictions based on block sizes, implicit transform can be applied only when LFNST and Matrix-based Intra Prediction (MIP) [34] indices are set to zero [38].

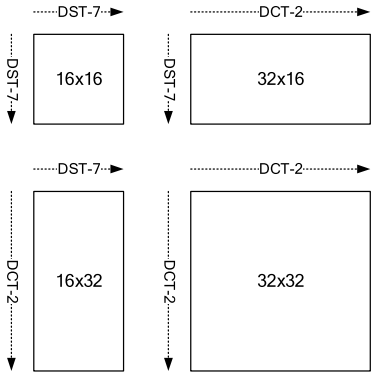

Fig. 2. Examples of transform type selection for vertical and horizontal transforms based on the implicit MTS in VVC.

The benefits of implicit MTS are summarized as follows: (1) Although implicit MTS provides less coding gain as compared to explicit MTS, it provides significant coding gain over DCT-2 without any encoder search. This feature is appealing for simple encoder designs that cannot accommodate a complex rate-distortion search. (2) Implicit MTS provides a unified transform derivation rule for both ISP coded and non-ISP intra coded blocks. (3) Since DST-7 is not allowed for dimensions beyond 16 in implicit MTS, the built-in zeroing out operation on high-frequency coefficients (which only applies for 32-point DST-7) is avoided.

B. Secondary Transform

The LFNST [39], [40] is a non-separable transform which applies to the top-left low-frequency region of primary transform coefficients, as shown in Figure 3. In VVC, the LFNST can be applied for intra coded blocks that use DCT-2 as the primary transform [41]. The transform kernels defined in LFNST consists of 4 transform sets with 2 kernels per set, where each kernel is selected among 48×16 and 16×16 matrices depending on transform block size. Specifically, a 48×16 kernel is applied to the top-left 8×8 region when a transform block (TB) is greater than or equal to 8×8, denoted as LFNST8, and a 16×16 kernel is applied to the top-left 4×4 region when TB width or height is 4, denoted as LFNST4. Detailed design of LFNST8 and LFNST4 is elaborated in next subsections.

1) LFNST Computation Process: The LFNST is computed in the form of matrix multiplication that is friendly to parallelism. The main idea of LFNST, also known as Reduced Secondary Transform (RST) [40], is mapping an N dimensional

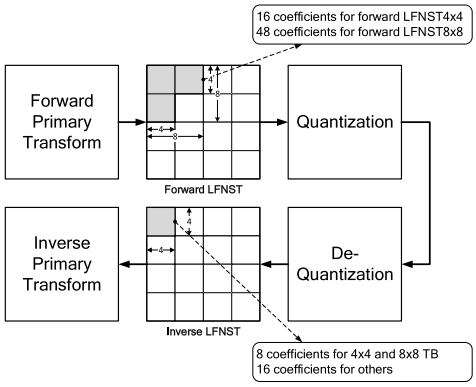

Fig. 3. Illustration of the LFNST design in VVC.

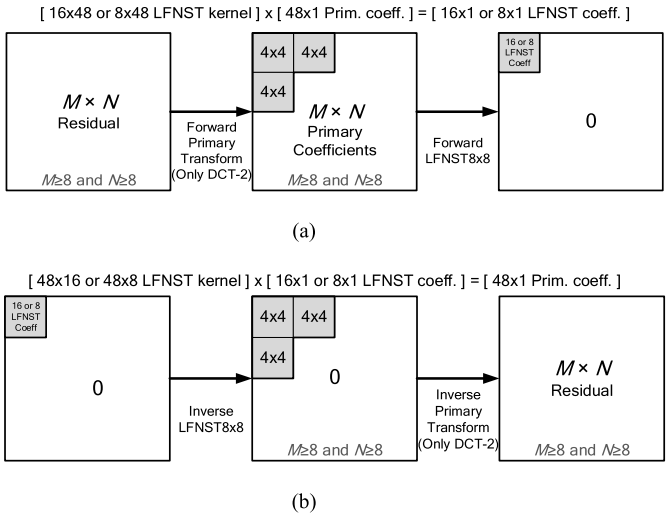

Fig. 4. The exemplary procedure of (a) forward LFNST8 and (b) backward LFNST8 with $16 \times 48/48 \times 16$ or sampled $8 \times 48/48 \times 8$ matrix.

TABLE III
THE LFNST SET SELECTION TABLE

intraPredMode	*lfnstSetIdx*
intraPredMode < 0	1
0 <= intraPredMode <= 1	0
2 <= intraPredMode <= 12	1
13 <= intraPredMode <= 23	2
24 <= intraPredMode <= 44	3
45 <= intraPredMode <= 55	2
56 <= intraPredMode <= 80	1

vector to an R dimensional vector through $R \times N$ matrix, where R is usually less than N where N/R is the reduction factor. The reduced $R \times N$ matrix is used as the kernel in a forward transform, which consists of R orthonormal row vectors of the N dimensional space, and its transposed matrix is used as the kernel in the inverse LFNST. The larger reduction factor indicates more complexity reduction in terms of computation and memory usage, which will be detailed in Section V.

The LFNST design in VVC employs two reduction factors to restrict the worst-case computation complexity to be 8 multiplications per sample and kernel memory to be 8KB. First, the LFNST8 has a reduction factor of 3 relative to square 48×48 matrix. With LFNST8, 48 coefficients from three pre-defined 4×4 blocks, namely Region of Interest for LFNST8 (ROI8), form the input vector that is multiplied by the 16×48 matrix to output 16 coefficients. For LFNST4, the Region of Interest, denoted as ROI4, is one single top-left 4×4 block. In addition, for 4×4 and 8×8 TBs, the LFNST design has an extra reduction factor of 2. That is, only the first 8 coefficients of the output vector are calculated. In this way, the worst-case multiplication count per sample is limited to be 8. It is observed that around 0.2% and 0.3% coding performance loss (i.e., BD-bitrates increase) are caused due to the reduction factor of 2 and the transform set reduction from 35 to 4, respectively.

The Figure 4(a) illustrates an example of applying forward LFNST8 with its 16×48 or sampled 8×48 matrix. When LFNST is applied, all primary transform coefficients other than ROI8 are zeroed out [42]. Then the output of LFNST8, which is a 16 or 8 coefficient vector, is further quantized and entropy coded [43]. For the case that only 8 output coefficients are generated, i.e. 4×4 or 8×8 TB, the coefficients after the 8^{th} position along the scanning order must be zero. Therefore, for coefficient coding, the last non-zero coefficient is coded with constraint that it is within the 8^{th} scanning position [43]. An example of applying inverse LFNST is shown in Figure 4(b). In the inverse LFNST8, given the input 16 or 8 LFNST coefficients, a 48×16 and a sampled 48×8 inverse LFNST matrix is used to perform the inverse LFNST and reconstruct the primary transform coefficients back to ROI8. Furthermore, LFNST is applied to both luma and chroma blocks for a dual tree, and LFNST indices for luma and chroma blocks are signalled separately. Otherwise, if the dual tree is disabled, a single LFNST index is signalled and used only for luma, because the LFNST is not applied to chroma in shared-tree case [44].

Regarding the interaction with ISP mode [34] in VVC, when there are multiple transform partitions in one intra coding unit, LFNST is applied to all transform blocks and a single LFNST index is signalled. The LFNST kernel was initially proposed to be 10-bit precision but it was quantized to 8-bit integer including sign. There was no noticeable coding performance impact due to this precision change.

2) LFNST Set Selection: An LFNST set indicates a group of transform kernel options that can be selected in LFNST. In VVC, four LFNST sets, denoted as *lfnstSetIdx*, are defined and the selection depends on the intra prediction mode, denoted as *intraPredMode*, as shown in Table III. In each LFNST set, three different options of LFNST kernel are provided and the selection is indicated by an LFNST index ranging from 0 to 2. If the LFNST index is equal to 0, LFNST is not applied. Otherwise, an LFNST is applied using one of the two kernels in the LFNST set and the selection is indicated by the LFNST index.

As mentioned above, an LFNST set is selected among 4 transform sets according to *intraPredMode*, which is derived from an original intra prediction mode. In addition, *lfnstSetIdx* is assigned to be 1 for negative values of *intraPredMode* in Table III, which corresponds to wide-angle intra prediction mode that is applied to cover the prediction angles beyond the diagonal prediction direction [34]. The basis images of

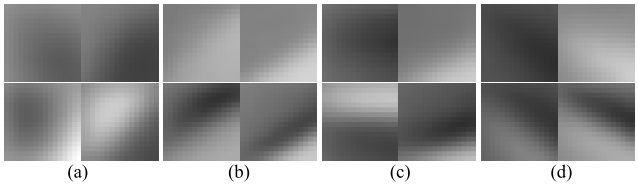

Fig. 5. First basis images of 16×16 DCT-2 and LFNST combinations. From left to right, (a) transform set 0, (b) transform set 1, (c) transform set 2 and (d) transform set 3.

16×16 DCT-2 and LFNST combination are shown in Figure 5, wherein the first basis images of four transform sets are shown in the first row and the second basis images of four transform sets are shown in the second row. Two columns of basis images are shown each transform set, corresponding to the two kernel candidates in one transform set. Here, the first and second basis refers to the basis that generates the first and second output LFNST coefficient, respectively. From Figure 5 it can be seen that, the directionality of basis images are well aligned with the associated intra prediction directionality, e.g., transform basis of transform set 1 show diagonal directionality.

There are two exceptions in the LFNST set selection process that are not defined solely by Table III. For a Cross-Component Linear Model (CCLM) mode, the wide angle intra prediction mode of collocated luma TB at the center position of the current chroma TB is used with Table III to select its LFNST set [45]. If MIP is applied and both width and height of the CU is greater than or equal to 16, LFNST set 0 is selected [46].

3) LFNST Index Signalling: LFNST index can be signalled for an intra-coded coding unit only when block width and height are greater than or equal to 4. On top of that, the following extra conditions are also considered to determine the LFNST signaling.

- If a non-zero coefficient is identified in zeroed-out region, it is not needed to signal an LFNST index since LFNST is inferred to be disabled in this case.
- If a non-zero coefficient exists only for DC position or it does not exist in any relevant color components, LFNST index signaling is skipped except for ISP mode.
- If one or more of all relevant color components is coded by transform skip, an LFNST index is not signalled [47].
- For a CU coded by MIP mode with either width or height being less than 16, LFNST is not signalled.
- If either width or height of a CU is greater than maximum transform size specified in SPS, LFNST is not signalled.

When an LFNST index is not signaled, it is inferred to be zero, i.e., LFNST is not applied.

C. Transform Partitioning

1) Sub-Block Transform: The distribution of inter-prediction residual is different from that of intra-prediction residual. Statistically, energy of inter-prediction residual increases from the center of prediction block towards its boundaries [48]. In addition, in many cases, the inter-prediction residuals are localized at one side of the block, rather than being distributed around all block boundaries. Inspired by the SVT [30] that uses a smaller transform block to capture the localized residuals, and further considering the unique distribution of inter-prediction residual, a Sub-Block Transform (SBT) method was developed and included in VVC.

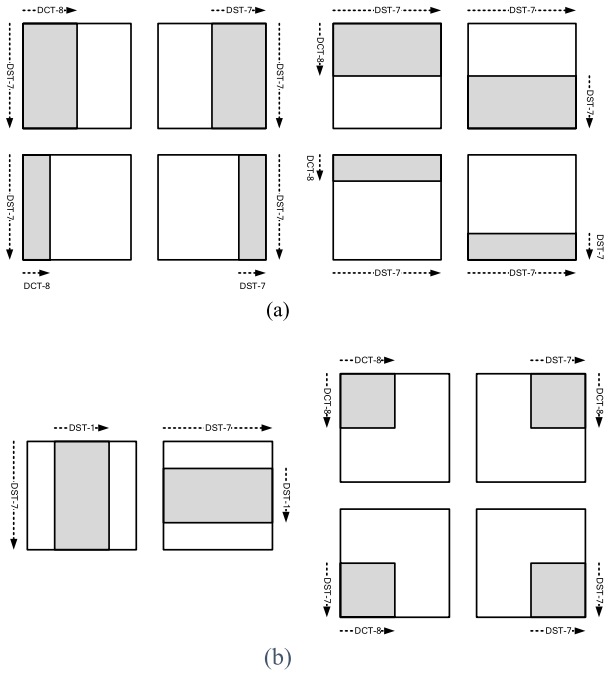

Fig. 6. Sub-block Transform modes (a) The eight SBT modes in VVC and (b) Additional SBT modes studied during VVC standardization.

In VVC, there are eight SBT modes associated with different configurations of the size and location of transform blocks. When SBT is used, the transform block is either half or quarter size of the residual block, as illustrated by the shaded blocks in Figure 6 (a), while residual in the rest part of the residual block is not coded and regarded as zero. In SBT, the transform blocks always reside in one boundary of the residual block.

Another feature of SBT design is the adaptive transform kernel, which is selected based on the transform block position, as illustrated in Figure 6 (a). This feature contributes to near half of the SBT coding gain [49]. If the residual is not evenly distributed within the residual block, the residual energy typically increases from one side to the other. For instance, if the transform block at the left side of the residual block is selected the best mode, the right side typically contains weaker residual. In this case, DCT-8 is more efficient than DCT-2 for the horizontal transform since the basis vector decreases from left to right. For the other dimension of the transform block, DST-7 is selected based on experimental results that show marginally higher coding gain than both DCT-2 and DCT-8.

During VVC standardization, another two types of SBT modes were proposed, as shown in Figure 6 (b). Each type contributes around 0.1% extra coding gain on top of the eight SBT modes that reflect the final design in VVC. The first type includes two modes, utilizing a half-sized transform block to cover the center of the residual block [50]. The transform block is coupled with type-1 DST (DST-1) in one dimension, because the associated basis vector has the highest value in the middle [20] which fits residual that is weaker at two sides of

the transform block than the center. Such a mode has smaller coding gain than each of the half-sized SBT modes with transform block locating at residual block boundaries. The second type includes four modes, with a quarter-sized transform block to cover one corner of the residual block [50]. The transform kernel selection is optimized based on the observation that residual increases from the center to a corner. In view of that the eight modes in Figure 6 (a) already contributed to the major coding gain, the six modes in Figure 6 (b) were not adopted in VVC, to avoid a more complicated SBT design as well as the introduction of an additional type of DST/DCT transform.

In a nutshell, the SBT modes are optimized for the cases that the major residual is localized at a lateral part of the residual block. During VVC standardization, transform unit split with position-dependent transform kernels were also studied for comparison with SBT, which showed marginally coding gain over SBT (especially on top of inter MTS) but required twice extra encoding runtime than SBT [51] for RDO.

For implementation consideration, when the width or height of an SBT transform block exceeds 32 (e.g., a 64×64 CU with any SBT mode), both horizontal and vertical transforms are forced to be DCT-2. In this way, it is aligned with the design principle in VVC that DST-7/DCT-8 is only applied to blocks no larger than 32×32.

2) Implicit Transform Partitioning: In VVC, the transform size can be up to 64-point, which is supported by DCT-2 only. The maximum transform size is selectable at sequence level and the transform size can be either 32 or 64-point [52]. When the coding unit width (or height) is greater than the maximum transform size, the prediction residual block will be further split horizontally (or vertically) into multiple transform blocks with width (or height) equal to maximum transform size. For one example, when the coding block size is 128×64 and the maximum transform size is 32-point, the coding block will be split into 8 transform units arranged in 4 rows and 2 columns. For another example, when the coding block size is 64×16 and the maximum transform size is 32-point, the coding block will be split into 2 transform units distributed horizontally with each transform unit covering a 32×16 residual block. The implicit transform splitting is processed with always vertical splitting first if the coding block width is greater than the maximum transform size. The transform splitting is done in a way that the coding order of transform units does not cross the 64×64 boundary. That is, all transform units within one 64×64 block are coded before any other transform unit in the next 64×64 block. In this way, the processing of transform units will not break down the VPDU implementation.

The signalling on maximum transform size provides the flexibility for encoder to implement up to either 32-point or 64-point transform size without limiting the coding block size. In addition, in VVC, lossless coding is achieved by enabling transform skip mode, which is supported by up to 32×32 block size. Therefore, with the option of selecting 32×32 as the maximum transform block size, coding block size greater than 32×32 can be also enabled for lossless coding. Furthermore, 64-point transform in VVC is always accompanied with zeroing out of the high frequencies, which may potentially create subjective quality artifacts. Maximum 32-point transform provides an alternate way of keeping large coding block without dropping any high frequency coefficients.

IV. Encoder Implementation in VTM

An efficient encoder algorithm is important in a practical video codec. In this section, to provide some insights on the encoder side design, the implementation of transform tools in VTM is described.

A. Encoder Decision for MTS and LFNST

In this section, MTS encoder implementation in VTM-9.0 is described. The transform using DCT-2 as both horizontal and vertical transform is checked first, then Transform Skip (TS) is evaluated, and DST-7 and DCT-8 are checked in the last. To achieve a reasonable coding gain versus complexity trade-off, a subset of transform candidates is first selected based on the cost measured by the L1-norm of a transform coefficient block, then the selected candidates are further evaluated based on high-complexity RD cost measurement. Specifically, if L1-norm of a transform candidate is less than or equal to a pre-determined threshold, the candidate is included in the candidate list for next high-complexity RD cost measurement if the list is not full. All the candidates enter the list in a first-in, first-out fashion if the cost is less than or equal to the given threshold. The maximum number of entries in the candidate list can be specified default VTM configuration files.

Since LFNST is only enabled when DCT-2 is applied as the primary transform, the encoder search of LFNST and MTS is jointly optimized using following two steps.

- *Step 1:* A predefined reduced set of transform modes is evaluated first, which includes DCT-2, TS, DST-7 and combination of DCT-2 and LFNST. Based on the evaluation outcome, the remaining MTS modes may be skipped.
- *Step 2:* If the remaining MTS modes are further checked, based on the outcome, it is further determined if the encoder search is terminated after checking a certain MTS mode.

As an exception to the above encoder process, combinations of ISP and LFNST are searched in addition to the checking DCT-2 pair or transform skip with LFNST off. Moreover, as aforementioned, ISP employs implicit MTS only. These two exceptions facilitate useful early skip decisions in VTM.

B. Sub-Block Transform (SBT)

SBT modes are searched after the regular DCT-2 transform for entire-block residual. A full search on all the eight SBT modes imposes significant encoder complexity, e.g., over 60% encoding time increase on VTM-3.0 under Random-Access configuration. Three fast algorithms have been developed to reduce the encoding time increase to around 8%, with less than 0.1% Bjøntegaard delta bitrates (BDR) penalty [53].

Algorithm 1: Based on residual energy distribution, certain SBT modes are skipped from encoder checking. Before performing transform and quantization, the RD cost for each

SBT mode is estimated using the signaling bits for the CU and the distortion of both the residual-skipped part and the residual-coded part, measured by sum of squared difference. If the estimated RD cost is already greater than the best RD cost (i.e., the minimum RD cost for the CU that is found before this prediction mode), the corresponding SBT mode is skipped further testing. In addition, at most four SBT modes are tested for any inter prediction mode.

Algorithm 2: When the prediction residual is either too large or too small, all SBT modes are skipped. More specifically, an inter prediction mode is unlikely to be chosen if its RD cost associated with full size transform exceeds the best RD cost to some extent. On the other hand, when the residual is too small, SBT is less efficient than skipping the residual due to the signaling overhead.

Algorithm 3: To decide from a large number of inter prediction modes and flexible coding tree as defined in VVC, a block may be encoded many times by different coding modes. After a residual block is encoded, the residual energy and the best transform mode among all candidates, i.e., the DCT-2 mode, inter MTS modes, and SBT mode, are recorded as a pair of historical information. When this region is encoded with another inter prediction mode, if the residual energy is similar to a recorded case, only the recorded best transform mode is tested for this prediction block. If a matching prior is not found, above fast algorithms 1 and 2 are invoked and later, the best transform mode after RDO is saved for later encoder decision.

V. Complexity Analysis

A. Primary Transform

As mentioned in Section III-A, high-frequency DCT-2 transform coefficients are zeroed out for the transform blocks with size (width and/or height) equal to 64, so that only the 32 low frequency coefficients are retained. For example, for an $M \times N$ transform block, when M is equal to 64, only the left 32 columns of transform coefficients are kept. Similarly, when N is equal to 64, only the top 32 rows of transform coefficients are kept. In addition, for 32-point DST-7 and DCT-8, only the 16 low frequency transform coefficients are kept and others are zeroed-out to reduce computation complexity [31]. With the zeroing-out, multiplication count is reduced to 37.5% for both 64-point DCT-2 and 32-point DST-7/DCT-8 for 64 $\times$ 64 and 32 $\times$ 32 transform blocks, respectively. Moreover, memory usage for 64-point DCT-2 and 32-point DST-7/DCT-8 is reduced to a half since only half of transform basis vectors are involved in the transform process. The multiplication counts per sample for all combinations of transform kernels and block shapes are summarized in Table IV.

In Table IV, M, N, m, and n denote TB width, TB height, width and height of top-left non-zero coefficients region, respectively. The analysis in Table IV is based on assumption that DCT-2 is computed using a partial butterfly structure [11]. When performing inverse transform, the vertical transform is performed first with the top-left m by n non-zero coefficient region as input and the output is an $M \times N$ block with only the left $m \times N$ region being nonzero. Then the horizontal transform is performed, and the output is an $M \times N$ residual block. During this transform process, only the multiplication counts associated with non-zero inputs were calculated, using the following formula, where N_{mul} is the total number of multiplication operations needed for a 2-D transform.

TABLE IV

The Multiplication Counts per Sample for All Combinations of Primary Transform Kernels and Block Shapes

M	N	DCT-2	DCT-2 w/o zero-out	DST-7 /DCT-8	DST-7 /DCT-8 w/o zero-out	LFNST +DCT-2
4	4	3.0	3.0	8.0	8.0	11.0
4	8	4.3	4.3	12.0	12.0	10.9
4	16	6.9	6.9	20.0	20.0	6.8
4	32	12.2	12.2	20.0	36.0	4.8
4	64	12.2	22.8	N/A	N/A	3.8
8	4	4.3	4.3	12.0	12.0	10.1
8	8	5.5	5.5	16.0	16.0	10.8
8	16	8.1	8.1	24.0	24.0	10.8
8	32	13.4	13.4	24.0	40.0	7.8
8	64	13.4	24.1	N/A	N/A	6.3
16	4	6.9	6.9	20.0	20.0	5.7
16	8	8.1	8.1	24.0	24.0	9.7
16	16	10.8	10.8	32.0	32.0	6.7
16	32	16.1	16.1	32.0	48.0	5.2
16	64	16.0	26.7	N/A	N/A	4.4
32	4	12.2	12.2	18.0	36.0	3.5
32	8	13.4	13.4	20.0	40.0	6.2
32	16	16.1	16.1	24.0	48.0	4.7
32	32	21.4	21.4	24.0	64.0	3.9
32	64	21.4	32.0	N/A	N/A	3.5
64	4	11.4	22.8	N/A	N/A	2.4
64	8	12.0	24.1	N/A	N/A	4.4
64	16	13.4	26.7	N/A	N/A	3.7
64	32	16.0	32.0	N/A	N/A	3.3
64	64	16.0	42.7	N/A	N/A	3.1

$$N_{\text{mul}} = \begin{cases} \dfrac{C_N}{N \cdot r_M \cdot r_N} + \dfrac{C_M}{M \cdot r_M} & \text{for DCT} - 2 \\ \dfrac{mn}{M} + m & \text{for DST} - 7/\text{DCT} - 8, \end{cases} \tag{4}$$

$$C_N = \frac{N^2 + 2}{3}, \quad r_N = \frac{N}{n}, \text{ and } r_M = \frac{M}{m}, \tag{5}$$

In Equation (4) and (5), C_N corresponds to the multiplication count for a one-dimensional N-point DCT-2. Without performing zeroing-out for 32-point DST-7/DCT-8, i.e., m equals to M and n equals to N, the worst-case multiplication counts for 32-point DST-7/DCT-8 becomes 64, as shown in Table IV, which is excessive for hardware implementation. For 64-point DCT-2, by zeroing out, more than half of multiplication counts is reduced. The coding performance impact from skipping high frequencies was observed to be around 0.1% and 0.05% bit-rate increase for AI and RA, respectively [31].

The memory usage of different transform types and sizes are summarized in Table V measured in bytes. In both HEVC and VVC, the smaller DCT-2 kernel can be sampled from larger one. In certain implementation, with this feature, the memory usage of DCT-2 with different sizes is same to the 64-point DCT-2, i.e. 2048 bytes. Furthermore, the DCT-8 basis vector can be derived by arranging the DST-7 basis in reverse order with sign value being alternated over all basis vectors [54]. Hence, DCT-8 can be derived from DST-7 without extra memory cost.

TABLE V
THE MEMORY USAGE INFORMATION OF ALL OF VVC PRIMARY TRANSFORM KERNELS (IN BYTES)

Transform	Length					Row sum
	4	8	16	32	64	
DCT-2	16	64	256	1,024	2,048	3,408
DST-7	16	64	256	512	N/A	848
DCT-8	16	64	256	512	N/A	848
Col. sum	48	192	768	2,048	2,048	5,104

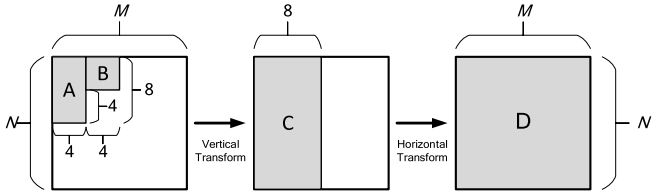

Fig. 7. The non-zero coefficient block expansion of primary transform from coefficients generated by inverse LFNST.

B. Secondary Transform

In the initial design of Reduced Secondary Transform (RST) [40], which is a previous version of LFNST, there are 35 transform sets. Each transform set is composed of 3 kernels except for Planar and DC modes that 2 kernels are defined in the transform set. In addition, for 8×8 and larger block sizes, 16×64 transform matrices are used in RST. In LFNST, total 4 transform sets are specified with 2 kernels for each transform set. The transform matrix dimensions of LFNST are 48×16 and 16×16 for LFNST8 and LFNST4, respectively. Moreover, the required worst-case number of multiplications per sample is 8, and up to 8 non-zero LFNST coefficients are processed for 4×4 and 8×8 blocks with further reduced LFNST matrices sampled from the 8×16 LFNST4 and 8×48 LFNST8 transform matrices, respectively. By further zeroing-out primary coefficients [42] when LFNST is applied, only the first 16 or 8 LFNST coefficients are kept and all other coefficients are set as zeros. Therefore, the maximum number of final transform coefficients becomes only 16 or 8, and the latter case happens in case of 4×4 or 8×8 transform block. This zeroing-out not only reduces computation complexity but also decreases coefficient buffer storage, which will be detailed below.

In Table IV, the total multiplication counts with both LFNST and DCT-2 being applied are reported. Given the output of LFNST, which is the top-left 48 or 16 coefficients, the number of multiplications needed for inverse primary transform is analyzed as follows. As shown in Figure 7, the left 4×8 (region A in Figure 7) and its neighboring 4×4 (region B in Figure 7) are first fed into the inverse vertical transform to generate the first 4 and the next 4 columns of output, which together form the M × N with only left $8 \times N$ block being nonzero (region C in Figure 7). Then this $8 \times N$ block is fed into the inverse horizontal transform and the output is the M × N residual block, as indicated by region D in Figure 7. In this analysis, it is assumed that the DCT-2 computation is performed using partial butterfly structure. Based on the above analysis, the following Equation (6) can be obtained for deriving the multiplication counts for DCT-2 in the case of a combination of LFNST and DCT-2, where C_M, C_N, r_M, and r_N are the same as in Equation (4).

$$N_{\text{mul}} = 4 \cdot \frac{C_N}{r_N} + 4 \cdot \frac{C_N}{2 \cdot r_N} + N \cdot \frac{C_M}{r_M} \tag{6}$$

It is noted that the overall complexity of LFNST and DCT-2 combination is smaller than the worst case of only primary transform being applied.

VI. EXPERIMENTAL RESULTS

A. Coding Efficiency

In this section, the coding performance of MTS (the explicit MTS), LFNST, SBT and 64-point DCT-2 are studied using the reference software VTM-9.0. The common test conditions (CTC), as defined by JVET for evaluating technical contributions during the standardization process of VVC, are used to perform the experiments. The test set defined in CTC includes a set of 32 video sequences, ranging from WQVGA (416×240) to 4K (3840×2160) resolutions, including four sequences with synthetic content, e.g., screen content, gaming content and mixed natural and screen content. The Bjøntegaard-delta rate (BDR) [53] is used to evaluate the coding performance. The tested quantization parameters (QP) are 22, 27, 32 and 37. The test conditions include All Intra (AI), Random Access (RA) and Low Delay B (LDB) as defined in the configuration files associated with the reference software VTM-9.0.

When evaluating the run-time difference, the following ΔT measurement is used,

$$\Delta T = \frac{T_{Proposed}}{T_{Anchor}} \times 100\%, \tag{7}$$

where T_{Anchor} and T_{Proposed} represent the runtimes of the anchor and proposed method. This criterion is used to estimate algorithm complexity in terms of encoder and decoder software run-time, where 100% indicates no run-time difference. To evaluate the overall BDR for multiple color components, an overall PSNR value derived as the sum of weighted luma and chroma PSNR values. The weights are 6/8, 1/8 and 1/8 for the PSNR value of Y, Cb and Cr components, respectively. These set of weights have been used in JVET for tool reporting [55].

When evaluating the coding performance, i.e., BDR, the anchor used in the results is VTM-9.0 with one (or multiple) tool(s) being disabled, and the test is VTM-9.0. For example, when reporting the coding gain of MTS, the anchor is VTM-9.0 with MTS being disabled (MTS = 0). Therefore, a negative BDR number indicates a bitrate reduction, i.e., coding gain.

The coding performance and software run-time of MTS and LFNST are reported in Table VI. For AI configuration, the average coding gains of MTS and LFNST are −1.25% and −1.19%, respectively. For RA configuration, the average gains of MTS and LFNST are −0.73% and −0.74%, respectively. The encoding run-time is approximately reduced by 10% when LFNST is enabled. One of main reasons is

TABLE VI
CODING GAIN OF MTS AND LFNST FOR AI AND RA CONFIGURATIONS IN CTC

Resolution	Sequences	All Intra						Random Access					
		MTS			LFNST			MTS			LFNST		
		BDR	ΔT_{Enc}	ΔT_{Dec}	BDR	ΔT_{Enc}	ΔT_{Dec}	BDR	ΔT_{Enc}	ΔT_{Dec}	BDR	ΔT_{Enc}	ΔT_{Dec}
Class A1	Tango2	-1.29%	116%	105%	-2.75%	91%	97%	-0.57%	104%	100%	-1.43%	105%	99%
	FoodMarket4	-1.92%	112%	103%	-2.03%	90%	99%	-0.81%	104%	100%	-1.07%	106%	100%
	Campfire	-0.84%	118%	101%	-0.56%	97%	102%	-0.68%	106%	100%	-1.18%	107%	100%
Class A2	CatRobot1	-1.43%	118%	104%	-1.23%	93%	101%	-0.55%	105%	99%	-0.83%	105%	100%
	DaylightRoad2	-1.43%	120%	101%	-0.76%	92%	99%	-0.53%	104%	99%	-0.72%	103%	99%
	ParkRunning3	-1.31%	118%	107%	0.02%	101%	106%	-0.94%	110%	101%	-0.07%	109%	100%
Class B	MarketPlace	-2.05%	123%	109%	-0.34%	92%	104%	-1.12%	108%	105%	-0.18%	106%	103%
	RitualDance	-1.77%	115%	107%	-1.11%	91%	105%	-1.20%	108%	105%	-0.55%	108%	104%
	Cactus	-1.54%	121%	105%	-0.97%	93%	104%	-0.86%	109%	104%	-0.72%	107%	102%
	BasketballDrive	-0.85%	117%	105%	-1.30%	89%	102%	-0.58%	108%	106%	-0.99%	107%	105%
	BQTerrace	-0.80%	122%	106%	-0.90%	90%	106%	-0.63%	108%	105%	-0.77%	105%	103%
Class C	BasketballDrill	-0.66%	115%	102%	-3.13%	89%	103%	-0.65%	111%	102%	-1.60%	108%	102%
	BQMall	-1.10%	118%	103%	-0.69%	90%	103%	-0.71%	109%	102%	-0.13%	106%	101%
	PartyScene	-0.59%	121%	106%	-0.38%	91%	104%	-0.51%	110%	102%	-0.11%	107%	102%
	RaceHorses	-0.88%	121%	108%	-1.00%	93%	105%	-0.57%	109%	103%	-0.74%	106%	101%
Class D	BasketballPass	-0.82%	116%	101%	-1.18%	93%	99%	-0.56%	109%	102%	-0.59%	108%	102%
	BQSquare	-0.46%	121%	101%	-0.44%	90%	99%	-0.32%	108%	99%	-0.59%	106%	99%
	BlowingBubbles	-0.62%	120%	99%	-0.92%	92%	100%	-0.43%	110%	101%	-0.31%	108%	101%
	RaceHorses	-0.86%	121%	103%	-1.49%	93%	101%	-0.52%	110%	104%	-0.71%	107%	102%
Class E	FourPeople	-1.56%	118%	108%	-1.19%	89%	105%						
	Johnny	-1.16%	117%	106%	-1.46%	87%	102%						
	KristenAndSara	-1.40%	117%	105%	-1.63%	88%	101%						
Class A1		-1.35%	115%	103%	-1.78%	93%	99%	-0.69%	105%	100%	-1.23%	106%	99%
Class A2		-1.39%	119%	104%	-0.65%	96%	102%	-0.68%	107%	100%	-0.54%	106%	100%
Class B		-1.40%	120%	106%	-0.92%	91%	104%	-0.88%	108%	105%	-0.64%	107%	103%
Class C		-0.81%	119%	105%	-1.30%	91%	104%	-0.61%	110%	102%	-0.65%	107%	101%
Class D		-0.69%	119%	101%	-1.01%	92%	100%	-0.46%	109%	102%	-0.55%	107%	101%
Class E		-1.37%	117%	106%	-1.43%	88%	103%						
Total Average*		**-1.25%**	**118%**	**105%**	**-1.19%**	**91%**	**103%**	**-0.73%**	**108%**	**102%**	**-0.74%**	**106%**	**101%**

*Average results do not include Class D

that, two different MTS encoding procedures are applied depending on the enabling of LFNST, and heavier MTS encoding procedure is applied when LFNST is turned off, which is detailed in Section IV. The combined coding gains of MTS and LFNST are also shown in Table VIII, and it is noted that the combined coding gain of MTS and LFNST is greater than the sum of individual coding gains, i.e., -3.52% and -1.91% for AI and RA configurations, respectively. This indicates that MTS and LFNST has some overlap on the coding gain, which is expected since both coding tools introduce additional transform kernels in a similar fashion as competing transform modes.

The results for SBT are reported in Table VII, the average gains for RA and LDB are -0.31% and -0.44%, respectively. With more advanced inter prediction and block partition in VVC, the inter prediction residue is greatly reduced, especially for RA, which leaves less room for SBT as well as other transform tools like inter MTS. Compared with inter MTS, SBT showed 0.3% higher coding gain in LDB with 40% of encoding runtime on VTM-3.0 [50], and achieved the best tradeoff between coding gain and encoding complexity among all transform tools for inter residual during VVC standardization.

The combined coding gains of MTS, LFNST and SBT, are reported in Table IX. Only RA and LDB results are reported since SBT only has an impact for those two test configurations. The combined coding gains of all transform coding techniques, including 64-point transform, MTS, LFNST and SBT, are also reported in Table X, and -4.5%, -3.6% and -2.2% are achieved for AI, RA and LDB configurations, respectively. The run-time impact of 64-point transform is very minor and not shown in this paper due to page limitations.

TABLE VII
CODING GAIN OF SBT FOR RA AND LDB CONFIGURATIONS IN CTC

Sequences	Random Access			Low Delay		
	BDR	ΔT_{Enc}	ΔT_{Dec}	BDR	ΔT_{Enc}	ΔT_{Dec}
Tango2	-0.04%	104%	99%			
FoodMarket4	-0.11%	103%	99%			
Campfire	-0.17%	105%	99%			
CatRobot1	-0.18%	105%	99%			
DaylightRoad2	-0.41%	106%	100%			
ParkRunning3	-0.72%	111%	100%			
MarketPlace	-0.32%	107%	101%	-0.50%	111%	99%
RitualDance	-0.36%	105%	101%	-0.47%	108%	104%
Cactus	-0.29%	106%	100%	-0.53%	110%	101%
BasketballDrive	-0.24%	106%	100%	-0.51%	110%	96%
BQTerrace	-0.47%	110%	101%	-0.82%	115%	100%
BasketballDrill	-0.19%	105%	101%	-0.31%	107%	98%
BQMall	-0.48%	106%	101%	-0.63%	110%	97%
PartyScene	-0.35%	106%	102%	-0.56%	111%	96%
RaceHorses	-0.38%	107%	102%	-0.53%	111%	100%
BasketballPass	-0.43%	106%	102%	-0.61%	110%	98%
BQSquare	-0.21%	105%	102%	-0.61%	109%	100%
BlowingBubbles	-0.36%	107%	102%	-0.55%	113%	101%
RaceHorses	-0.40%	108%	102%	-0.64%	112%	102%
FourPeople				-0.28%	105%	98%
Johnny				-0.01%	103%	100%
KristenAndSara				-0.18%	104%	99%
Class A1	-0.11%	104%	100%			
Class A2	-0.44%	107%	100%	-0.56%	111%	101%
Class B	-0.34%	108%	106%	-0.51%	112%	113%
Class C	-0.35%	106%	103%	-0.60%	112%	108%
Class D	-0.35%	107%	102%	-0.16%	105%	108%
Class E				-0.20%	106%	106%
Total Average*	**-0.31%**	**106%**	**100%**	**-0.44%**	**109%**	**99%**

*Average results do not include Class D

TABLE VIII

CODING GAIN OF MTS + LFNST FOR AI AND RA CONFIGURATIONS IN CTC

Sequences	All Intra			Random Access		
	BDR	ΔT_{Enc}	ΔT_{Dec}	BDR	ΔT_{Enc}	ΔT_{Dec}
Class A1	-4.67%	163%	103%	-2.54%	116%	100%
Class A2	-3.11%	172%	107%	-1.60%	115%	101%
Class B	-3.28%	172%	107%	-2.03%	117%	104%
Class C	-2.74%	170%	103%	-1.54%	118%	102%
Class E	-4.20%	164%	105%			
Total Average*	**-3.52%**	**169%**	**105%**	**-1.91%**	**117%**	**102%**

TABLE IX

COMBINED CODING GAIN OF MTS, LFNST AND SBT FOR AI, RA AND LDB CONFIGURATIONS IN CTC

	Random Access			Low Delay		
	BDR	ΔT_{Enc}	ΔT_{Dec}	BDR	ΔT_{Enc}	ΔT_{Dec}
Class A1	-2.60%	122%	100%			
Class A2	-1.83%	124%	100%			
Class B	-2.22%	126%	104%	-0.94%	113%	100%
Class C	-1.76%	127%	108%	-0.84%	114%	105%
Class E				-0.42%	106%	102%
Average	**-2.10%**	**125%**	**103%**	**-0.77%**	**112%**	**102%**

TABLE X

COMBINED CODING GAIN OF 64-POINT TRANSFORM, MTS, LFNST AND SBT FOR AI, RA AND LDB CONFIGURATIONS IN CTC

	All Intra	Random Access	Low Delay
Class A1	-7.12%	-6.65%	
Class A2	-4.06%	-3.17%	
Class B	-4.08%	-3.41%	-2.76%
Class C	-2.87%	-2.04%	-1.32%
Class E	-5.28%		-2.31%
Average	**-4.51%**	**-3.65%**	**-2.17%**

B. Tool Analysis

In Figure 8, the coding blocks using MTS, LFNST and SBT are highlighted using red, blue and green boxes, respectively. The above one is the first reconstructed picture (Intra frame) of BQTerrace (1920×1080), and the bottom one is the third reconstructed picture (B frame) of MartketPlace (1920×1080). Those pictures are reconstructed using bitstream coded by VTM-9.0 following the CTC under RA configuration using QP 37 (BQTerrace) and 27 (MarketPlace). It is observed that MTS and LFNST coded blocks cover a considerable percentage of blocks in Intra frame coding. However, for blocks with smooth or vertical texture patterns (top-left part of the picture), neither MTS nor LFNST is used frequently. These blocks typically show little specific residual patterns, where separable transform using DCT-2 seems to be efficient. For Inter coding, it is observed that SBT is more frequently used along the moving object boundaries. This represents a typical case where SBT can be helpful, since the residual can be more frequently locally distributed within one coding block.

From Table VI and Table VII, it is noticed that MTS and SBT contribute relatively consistent coding gain across different video content and resolutions, while the coding gain of LFSNT is higher for an input sequence with rich directional texture patterns (BasketballDrill) of which coding gain can go up to 3% for AI coding configuration. For SBT, from Table VII, it is noted that the coding gain is consistent across different resolutions, and for sequences with complex motion, and frequent object occlusions (ParkRunning3), the RA coding gain of SBT is peaked at 0.7%.

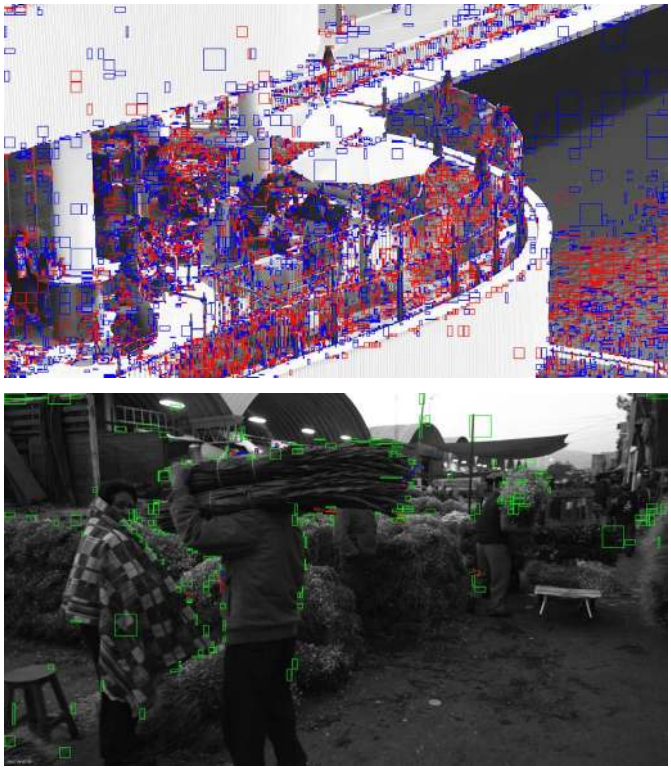

Fig. 8. Reconstructed picture of BQTerrace (top) and MarketPlace (bottom) with coding blocks selecting MTS, LFNST and SBT highlighted in red, blue and green, respectively.

VII. CONCLUSION

The transform coding design for VVC has been described in this paper, including new primary transform kernel types with explicit and implicit selection schemes, explicitly signalled non-separable secondary transform with reduced kernels and sub-block transform partitioning. Besides these new transform tools, VVC also extended several aspects of the HEVC transform design, including 64-point DCT-2 and transform for rectangular block shape. Moreover, normative zeroing-out schemes are applied in VVC for 64-point DCT-2, 32-point DST-7/DCT-8 and LFNST to reduce complexity. Experimental results show significant coding gains contributed by MTS, LFNST, SBT and 64-point DCT-2, especially for intra coding with up to 7.1% BD rate reduction for 4K video contents.

REFERENCES

[1] *Video Codec for Audiovisual Services at P x 64 kbit/s*, document ITU-T Rec. H.261, Dec. 1990.

[2] *Information Technology-Coding of Moving Pictures and Associated Audio for Digital Storage Media at up to About 1.5 Mbit/s: Video*, document ISO/IEC 11172-2 MPEG-1, 1993.

[3] *Information Technology-Generic Coding of Moving Pictures and Associated Audio Information: Video*, document ITU-T Rec. H.262 and ISO/IEC 13818-2 MPEG-2, 1995.

[4] *Video Coding for Low Bitrate Communication*, document ITU-T Rec. H.263 Version 1, 1995, Version 2, Sep. 1997.

[5] T. Wiegand, G. J. Sullivan, G. Bjontegaard, and A. Luthra, "Overview of the H.264/AVC video coding standard," *IEEE Trans. Circuits Syst. Video Technol.*, vol. 13, no. 7, pp. 560–576, Jul. 2003.

[6] G. J. Sullivan, J.-R. Ohm, W.-J. Han, and T. Wiegand, "Overview of the high efficiency video coding high efficiency video coding standard," *IEEE Trans. Circuits Syst. Video Technol.*, vol. 22, no. 12, pp. 1649–1668, Dec. 2012.

[7] N. Ahmed, T. Natarajan, and K. R. Rao, "Discrete cosine transform," *IEEE Trans. Comput.*, vol. C-23, no. 1, pp. 90–93, Jan. 1974.

[8] K. Karhunen, *Über Lineare Methoden in der Wahrscheinlichkeitsrechnung* (Annales Academiae scientiarum Fennicae. Series A. 1, Mathematica-Physica), no. 37. 1947, pp. 1–79.

[9] W.-H. Chen, C. Smith, and S. Fralick, "A fast computational algorithm for the discrete cosine transform," *IEEE Trans. Commun.*, vol. COM-25, no. 9, pp. 1004–1009, Sep. 1977.

[10] H. S. Malvar, A. Hallapuro, M. Karczewicz, and L. Kerofsky, "Low-complexity transform and quantization in H.264/AVC," *IEEE Trans. Circuits Syst. Video Technol.*, vol. 13, no. 7, pp. 598–603, Jul. 2003.

[11] M. Budagavi, A. Fuldseth, G. Bjontegaard, V. Sze, and M. Sadafale, "Core transform design in the high efficiency video coding standard," *IEEE J. Sel. Topics Signal Process.*, vol. 7, no. 6, pp. 1029–1041, Dec. 2013.

[12] B. Zeng and J. Fu, "Directional discrete cosine transforms—A new framework for image coding," *IEEE Trans. Circuits Syst. Video Technol.*, vol. 18, no. 3, pp. 305–313, Mar. 2008.

[13] B. Bross *et al.*, "Overview of the versatile video coding (VVC) standard and its applications," *IEEE Trans. Circuits Syst. Video Technol.*, to be published.

[14] K. Rose, A. Heiman, and I. Dinstein, "DCT/DST alternate-transform image coding," *IEEE Trans. Commun.*, vol. 38, no. 1, pp. 94–101, Jan. 1990.

[15] Y. Ye and M. Karczewicz, "Improved H.264 intra coding based on bi-directional intra prediction, directional transform, and adaptive coefficient scanning," in *Proc. 15th IEEE Int. Conf. Image Process.*, Oct. 2008, pp. 2116–2119.

[16] J. Han, A. Saxena, V. Melkote, and K. Rose, "Jointly optimized spatial prediction and block transform for video and image coding," *IEEE Trans. Image Process.*, vol. 21, no. 4, pp. 1874–1884, Apr. 2012.

[17] A. K. Jain, "A sinusoidal family of unitary transforms," *IEEE Trans. Pattern Anal. Mach. Intell.*, vol. PAMI-1, no. 4, pp. 356–365, Oct. 1979.

[18] X. Zhao, L. Zhang, S. Ma, and W. Gao, *Rate-Distortion Optimized Transform*, document ISO/IEC JTC1/SC29/WG11, m16926, Xi'an, China, Oct. 2009.

[19] S.-C. Lim *et al.*, "Rate-distortion optimized adaptive transform coding," *Opt. Eng.*, vol. 48, no. 8, Aug. 2009, Art. no. 087004.

[20] X. Zhao, J. Chen, M. Karczewicz, A. Said, and V. Seregin, "Joint separable and non-separable transforms for next-generation video coding," *IEEE Trans. Image Process.*, vol. 27, no. 5, pp. 2514–2525, May 2018.

[21] T. Biatek, V. Lorcy, and P. Philippe, "Transform competition for temporal prediction in video coding," *IEEE Trans. Circuits Syst. Video Technol.*, vol. 29, no. 3, pp. 815–826, Mar. 2019.

[22] A. Arrufat, P. Philippe, and O. Déforges, "Non-separable mode dependent transforms for intra coding in high efficiency video coding," in *Proc. IEEE Proc. Vis. Commun. Image Process.*, Dec. 2014, pp. 61–64.

[23] S. Takamura and A. Shimizu, "On intra coding using mode dependent 2D-KLT," in *Proc. Picture Coding Symp. (PCS)*, Dec. 2013, pp. 137–140.

[24] H. E. Egilmez, O. G. Guleryuz, J. Ehmann, and S. Yea, "Row-column transforms: Low-complexity approximation of optimal non-separable transforms," in *Proc. IEEE Int. Conf. Image Process. (ICIP)*, Sep. 2016, pp. 2385–2389.

[25] A. Saxena and F. C. Fernandes, "On secondary transforms for prediction residual," in *Proc. 19th IEEE Int. Conf. Image Process.*, Sep. 2012, pp. 2489–2492.

[26] X. Zhao, J. Chen, A. Said, V. Seregin, H. E. Egilmez, and M. Karczewicz, "NSST: Non-separable secondary transforms for next generation video coding," in *Proc. Picture Coding Symp. (PCS)*, Dec. 2016, pp. 1–5.

[27] A. Said, X. Zhao, M. Karczewicz, H. E. Egilmez, V. Seregin, and J. Chen, "Highly efficient non-separable transforms for next generation video coding," in *Proc. Picture Coding Symp. (PCS)*, Dec. 2016, pp. 1–5.

[28] M. Wien, "Variable block-size transforms for H.264/AVC," *IEEE Trans. Circuits Syst. Video Technol.*, vol. 13, no. 7, pp. 604–613, Jul. 2003.

[29] I.-K. Kim, J. Min, T. Lee, W.-J. Han, and J. Park, "Block partitioning structure in the high efficiency video coding standard," *IEEE Trans. Circuits Syst. Video Technol.*, vol. 22, no. 12, pp. 1697–1706, Dec. 2012.

[30] C. Zhang, K. Ugur, J. Lainema, A. Hallapuro, and M. Gabbouj, "Video coding using spatially varying transform," *IEEE Trans. Circuits Syst. Video Technol.*, vol. 21, no. 2, pp. 127–140, Feb. 2011.

[31] M. Koo, M. Salehifar, J. Lim, S. Kim, *CE6-Related: 32 Point MTS Based on Skipping High Frequency Coefficients*, document Joint Video Experts Team of ITU-T SG 16 WP 3 and ISO/IEC JTC 1/SC 29/WG 11, JVET-M0297, Marrakech, Morocco, Jan. 2019.

[32] X. Zhao *et al.*, *CE6: Fast DST-7/DCT-8 With Dual Implementation Support (Test 6.2.3)*, document Joint Video Experts Team of ITU-T SG 16 WP 3 and ISO/IEC JTC 1/SC 29/WG 11, JVET-M0497, Marrakech, Morocco, 2019.

[33] Z. Zhang *et al.*, "Fast DST-VII/DCT-VIII with dual implementation support for versatile video coding," *IEEE Trans. Circuits Syst. Video Technol.*, vol. 31, no. 1, pp. 355–371, Jan. 2021.

[34] J. Pfaff *et al.*, "Intra prediction and mode coding in VVC," *IEEE Trans. Circuits Syst. Video Technol.*, early access, Apr. 12, 2021, doi: 10.1109/TCSVT.2021.3072430.

[35] S. De-Luxán-Hernández *et al.*, *Non-CE6: Combination of JVET-P0196 and JVET-P0392 on Applying LFNST for ISP Blocks and Simplifying the Transform Signalling*, document Joint Video Experts Team of ITU-T SG 16 WP 3 and ISO/IEC JTC 1/SC 29/WG 11, JVET-P1026, Geneva, Switzerland, 2019.

[36] J. Lainema, *CE6-Related: Shape Adaptive Transform Selection*, document Joint Video Experts Team of ITU-T SG 16 WP 3 and ISO/IEC JTC 1/SC 29/WG 11, JVET-L0134, Macao, CN, USA, 2018.

[37] H. Gao *et al.*, *Non-CE6: Combined Test of JVET-N0172/JVET-N0375/JVET-N0419/JVET-N0420 on Unification of Implicit Transform Selection*, document Joint Video Experts Team of ITU-T SG 16 WP 3 and ISO/IEC JTC 1/SC 29/WG 11, JVET-N0866, Geneva, Switzerland, 2019.

[38] K. Naser, F. L. Léannec, T. Poirier, *Non-CE6 Interaction Between Implicit MTS and LFNST and MIP*, document Joint Video Experts Team of ITU-T SG 16 WP 3 and ISO/IEC JTC 1/SC 29/WG 11, JVET-O0529, Gothenburg, Sweden, 2019.

[39] M. Koo, M. Salehifar, J. Lim, and S.-H. Kim, "Low frequency non-separable transform (LFNST)," in *Proc. Picture Coding Symp. (PCS)*, Nov. 2019, pp. 1–5.

[40] M. Koo *et al.*, *CE6: Reduced Secondary Transform (RST) (CE6-3.1)*, document Joint Video Experts Team of ITU-T SG 16 WP 3 and ISO/IEC JTC 1/SC 29/WG 11, JVET-N0193, Geneva, Switzerland, 2019.

[41] M.-S. Chiang *et al.*, *CE6-related: Simplifications for LFNST*, document Joint Video Experts Team (JVET) of ITU-T SG 16 WP 3 and ISO/IEC JTC 1/SC 29/WG 11, JVET-O0292, Gothenburg, Sweden, Jul. 2019.

[42] M. Siekmann, H. Schwarz, D. Marpe, T. Wiegand, *CE6-2.1: Simplification of Low Frequency Non-Separable Transform*, document Joint Video Experts Team of ITU-T SG 16 WP 3 and ISO/IEC JTC 1/SC 29/WG 11, JVET-O0094, Gothenburg, Sweden, 2019.

[43] H. Schwarz *et al.*, "Quantization and entropy coding in the versatile video coding (VVC) standard," *IEEE Trans. Circuits Syst. Video Technol.*, early access, Apr. 9, 2021, doi: 10.1109/TCSVT.2021.3072202.

[44] H. E. Egilmez *et al.*, *Combination of JVET-Q0106, JVET-0686 and JVET-Q0133 for LFNST Signaling, Latency Reduction and Scaling Process*, document Joint Video Experts Team of ITU-T SG 16 WP 3 and ISO/IEC JTC 1/SC 29/WG 11, JVET-P0784, Brussels, Belgium, 2020.

[45] Z. Zhang *et al.*, *Non-CE6: On LFNST Transform Set Selection for a CCLM Coded Block*, document Joint Video Experts Team of ITU-T SG 16 WP 3 and ISO/IEC JTC 1/SC 29/WG 11, JVET-O0219, Gothenburg, Sweden, 2019.

[46] J. Pfaff *et al.*, *Non-CE3: Simplifications of MIP*, document Joint Video Experts Team of ITU-T SG 16 WP 3 and ISO/IEC JTC 1/SC 29/WG 11, JVET-O0925, Gothenburg, Sweden, 2019.

[47] B. Heng *et al.*, *AHG16: Combination of LFNST With Transform Skip*, document Joint Video Experts Team of ITU-T SG 16 WP 3 and ISO/IEC JTC 1/SC 29/WG 11, JVET-Q0106, Brussels, Belgium, 2020.

[48] J. An, X. Zhao, X. Guo, S. Lei, *Non-CE7: Boundary-Dependent Transform for Inter-Predicted Residue*, document Joint Collaborative Team on Video Coding (JCT-VC) of ITU-T SG16 WP3 and ISO/IEC JTC1/SC29/WG11, JCTVC-G281, Geneva, Switzerland, 2011.

[49] Y. Zhao, H. Yang, J. Chen, *CE6: Spatially Varying Transform (Test 6.1.12.1)*, document Joint Video Experts Team (JVET) of ITU-T SG 16 WP 3 and ISO/IEC JTC 1/SC 29/WG 11, JVET-K0139, Ljubljana, Slovenia, 2018.

[50] Y. Zhao, H. Gao, H. Yang, J. Chen,*CE6: Sub-Block Transform for Inter Blocks (Test 6.4.1)*, document Joint Video Experts Team of ITU-T SG 16 WP 3 and ISO/IEC JTC 1/SC 29/WG 11, JVET-M0140, Marrakech, Morocco, 2019.

[51] Y. Zhao *et al.*, *CE6: RQT-Like Sub-Block Transform for Inter Blocks (Test 6.4.4)*, document Joint Video Experts Team of ITU-T SG 16 WP 3 and ISO/IEC JTC 1/SC 29/WG 11, JVET-M0141, Marrakech, Morocco, 2019.
[52] X. Zhao, X. Li, S. Liu, *Non-CE6: Configurable Maximum Transform Size in VVC*, document Joint Video Experts Team of ITU-T SG 16 WP 3 and ISO/IEC JTC 1/SC 29/WG 11, JVET-O0545, Gothenburg, Sweden, 2019.
[53] G. Bjøntegaard, *Improvement of BD-PSNR Model*, document ITU-T SG16/Q6, Doc. VCEG-AI11, Berlin, Germany, 2008.
[54] M. Koo, M. Salehifar, J. Lim, S. Kim, *CE 6-1.11: AMT Replacement and Restriction*, document Joint Video Experts Team of ITU-T SG 16 WP 3 and ISO/IEC JTC 1/SC 29/WG 11, JVET-K0096, Ljubljana, Slovenia, 2018.
[55] W.-J. Chien *et al.*, *JVET AHG Report: Tool Reporting Procedure (AHG13)*, document Joint Video Experts Team of ITU-T SG 16 WP 3 and ISO/IEC JTC 1/SC 29/WG 11, JVET-S0013, 2020.

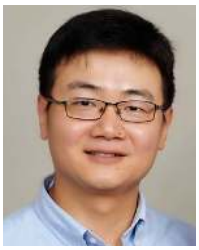

Xin Zhao (Senior Member, IEEE) received the B.S. degree in electronic engineering from Tsinghua University, Beijing, China, and the Ph.D. degree in computer applications from the Institute of Computing Technology, Chinese Academy of Sciences, Beijing. He was a Staff Engineer with Qualcomm, San Diego, CA, USA. In 2017, he joined Tencent, Palo Alto, CA, USA, where he is currently a Principal Researcher and the Manager of multimedia standards with Tencent Media Lab. He has been actively contributing to the development of multiple video standards for over ten years, such as HEVC and 3D extensions to H.264/AVC and HEVC, and VVC. He has contributed over 200 standard proposals and published over 30 journal articles and conference papers. His research interests include image and video coding, video processing, and transmission.

Seung-Hwan Kim received the Ph.D. degree from the Gwangju Institute of Science Technology (GIST) in 2008. In 2009, he was with the University of Southern California (USC), as a Post-Doctoral Research Fellow. In 2011, he joined Sharp Labs of America, where he has been active in video coding standardization in ITU-T and ISO/IEC for development of high-efficiency video coding (HEVC) and its extension projects, including joint video experts team (JVET). Since 2016, he has been with LGE U.S., where he is an Assistant Vice President and has lead versatile video coding (VVC) activity, as the Head of video codec part. His main research interests include image and video signal processing, data compression, pattern recognition, and machine learning.

Yin Zhao received the B.S. and Ph.D. degrees from Zhejiang University, Hangzhou, China, in 2008 and 2013, respectively. In 2013, he joined Huawei Technologies, Hangzhou, where he is currently a Technical Expert. Since 2017, he has been actively participating in the development of several video coding standards, including the H.266/VVC, AVS3, and MPEG-5 EVC standards. He designed and developed the sub-block transform and local dual tree in H.266/VVC. He has been one of the software coordinators of AVS3 test model. His research interests include video coding, quality assessment, and image processing.

Hilmi E. Egilmez (Member, IEEE) received the B.S. and M.Sc. degrees in electrical and electronics engineering from Koc University, Istanbul, Turkey, in 2010 and 2012, respectively, and the Ph.D. degree in electrical engineering from the University of Southern California, Los Angeles, USA, in 2017. He is currently with Qualcomm Technologies Inc., San Diego, USA. His research interests include the areas of signal processing, machine learning, and image/video coding.

Moonmo Koo received the B.S. and Ph.D. degrees in electrical and computer engineering from Seoul National University, Seoul, South Korea, in 2001 and 2011, respectively. In 2011, he joined LG Electronics Inc. Since then, he did projects for depth estimation and 3D view synthesis hardware designs and developed video coding algorithms, and has been participating in video coding standardization in ITU-T and ISO/IEC for development of Versatile Video Coding (VVC). His research interests include image/video compression, machine learning based video coding, and HW/SW system design for video applications.

Shan Liu (Senior Member, IEEE) received the B.Eng. degree in electronic engineering from Tsinghua University, and the M.S. and Ph.D. degrees in electrical engineering from the University of Southern California. She was the Director of the Media Technology Division at MediaTek, USA. She was also with MERL, Sony, and IBM. She is currently a Tencent Distinguished Scientist and the General Manager of Tencent Media Lab. She has been actively contributing to international standards since the last decade and served as a co-editor for HEVC SCC and the emerging VVC. She has numerous technical contributions adopted into various standards, such as HEVC, VVC, OMAF, DASH, and PCC. Technologies and products developed by her and under her leadership have served several hundred million users. She holds more than 150 granted U.S. and global patents and has published more than 80 journal articles and conference papers. Her research interests include audio-visual, high volume, immersive and emerging media compression, intelligence, transport, and systems.

Jani Lainema received the M.Sc. degree in computer science from the Tampere University of Technology, Finland, in 1996. He joined the Visual Communications Laboratory, Nokia Research Center, in 1996. Since 1996, he has been contributed to the designs of ITU-T's and MPEG's video coding standards and to the evolution of different multimedia service standards in 3GPP, DVB, and DLNA. He is currently a Bell Labs Distinguished Member of Technical Staff and a Distinguished Scientist in visual media at Nokia Technologies, Tampere, Finland. His research interests include video, image, and graphics coding and communications.

Marta Karczewicz received the M.Sc. and Ph.D. (Hons.) degrees from the Tampere University of Technology, Finland, in 1994 and 1997, respectively. From 1996 to 2006, she was with Nokia, where she managed "Visual Technologies" competence area and became the Head of Nokia Research Center, Dallas, TX, USA, in 2004. In 2006, she joined Qualcomm, where she is currently the Vice President of the Multimedia Research and Development Group. Since 1998, she has been an active participant in H.264/AVC, HEVC and VVC video codecs development within MPEG and ITU-T standardization forums. She holds over 300 granted U.S. and over 100 granted European patents on video compression. She has authored 15 journal articles and over 40 conference papers, including four invited papers to two special issues of the IEEE TRANSACTIONS ON CIRCUITS AND SYSTEMS FOR VIDEO TECHNOLOGY on AVC and HEVC. She received the 1996–1997 EURASIP's Best Paper Award in Image Communication category. She is one of the three Finalists for the 2019 European Inventor Award in the "Lifetime Achievement" category.